Targeted molecular imaging of head and neck squamous cell carcinoma: a window into precision medicine

Jun Wu, Ying Yuan, Xiao-Feng Tao

Department of Radiology, School of Medicine, Shanghai Ninth People's Hospital, Shanghai Jiao Tong University, Shanghai 200011, China.

Abstract

Tumor biomarkers play important roles in tumor growth, invasion, and metastasis. Imaging of specific biomarkers will help to understand different biological activities, thereby achieving precise medicine for each head and neck squamous cell carcinoma (HNSCC) patient. Here, we describe various molecular targets and molecular imaging modalities for HNSCC imaging. An extensive search was undertaken in the PubMed database with the keywords including "HNSCC," "molecular imaging," "biomarker," and "multimodal imaging." Imaging targets in HNSCC consist of the epidermal growth factor receptor, cluster of differentiation 44 variant 6 (CD44v6), and mesenchymal-epithelial transition factor and integrins. Targeted molecular imaging modalities in HNSCC include optical imaging, ultrasound, magnetic resonance imaging, positron emission tomography, and single-photon emission computed tomography. Making the most of each single imaging method, targeted multimodal imaging has a great potential in the accurate diagnosis and therapy of HNSCC. By visualizing tumor biomarkers at cellular and molecular levels *in vivo*, targeted molecular imaging can be used to identify specific genetic and metabolic aberrations, thereby accelerating personalized treatment development for HNSCC patients.

Keywords: Molecular imaging; Head and neck squamous cell carcinoma; Biomarker; Multimodal imaging

Introduction

Head and neck squamous cell carcinoma (HNSCC) is an epithelial malignancy that arises primarily from the oral cavity, oropharynx, hypopharynx, and larynx.[1] HNSCC is characterized by local tumor invasion, metastasis, early recurrence, and development of second primary tumors, which are the major causes of morbidity and mortality,[2] Unfortunately, conventional therapies (eg, surgery, radiotherapy, and chemotherapy) have several limitations and are not personalized to each patient.[3] The prognosis of HNSCC patients is poor, and the 5-year survival rate remains less than 65%.[4] Taking individual genetic variabilities into account, precision medicine can provide individually "tailored" therapeutic interventions that can improve the outcome of patients.[5] To a large extent, this strategy is dependent upon the availability of target-specific drugs and/or imaging agents that reveal patient-specific mechanisms in carcinogenesis.[6]

Molecular imaging is a real-time and non-invasive way to visualize the expression and activity of specific targets (cell-surface receptors or biomarkers) as well as biological processes (eg, angiogenesis or apoptosis) at molecular and cellular levels.[7] Conventional imaging modalities, such as ultrasound (US), computed tomography (CT), and conventional magnetic resonance imaging (MRI), can only provide anatomical information. However, molecular imaging enables dynamic and quantitative visualization of specific biochemical activity *in vivo*. Prostate-specific membrane antigen-targeted positron emission tomography (PET) imaging agents for prostate cancer or somatostatin receptor-targeted probes for imaging neuroendocrine tumors have been used widely in the clinic.[8,9] Some tumor receptors are related to the tumor proliferation and metastatic potential. By targeting these receptors, molecular imaging has been employed for early detection, identification of tumor margins, treatment planning, and accurate prediction of the prognosis of HNSCC; therefore, improving the outcomes of HNSCC patients.

Early detection of HNSCC is a major clinical issue. Unfortunately, only one-third of HNSCC patients are diagnosed at an early stage due to lack of symptoms.[10] HNSCC patients diagnosed at advanced stages (T3 or T4), require extensive resection or comprehensive cervical lymphadenectomy, which are associated with a poor quality of life.[11] Early diagnosis is attributed mainly to a

Access this article online

Quick Response Code:

Website: www.cmj.org

DOI: 10.1097/CM9.0000000000000751

Correspondence to: Prof. Xiao-Feng Tao, Department of Radiology, School of Medicine, Shanghai Ninth People's Hospital, Shanghai Jiao Tong University, 639 Zhizao Ju Road, Shanghai 200011, China
E-Mail: cjr.taoxiaofeng@vip.163.com

Chinese Medical Journal 2020;133(11)

Received: 09-02-2020 **Edited by:** Peng Lyu

lack of appropriate screening and diagnostic biomarkers.[12] Tissue biopsy is invasive and prone to sampling errors, which makes it inappropriate for early screening. Conventional imaging methods do not have sufficient resolution to detect microscopic (subclinical) disease. By visualizing expression of these biomarkers, targeted molecular imaging can be used for the early detection of HNSCC and provide accurate information about tumors, surrounding tissues, and its metastatic status, all of which are important for tumor staging and grading.[11,13]

Surgical resection is one of the primary treatment of choices. The extent of resection directly affects the outcome and prognosis of the patients. Positive margins are associated with increased local recurrence and indicate a poor prognosis for patients with HNSCC.[14] Thus, securing negative surgical margins is an important therapeutic goal.[15] Despite improvements in surgical oncology, accurate delineation of tumor margins is challenging.[16] Pre-operative MRI can be only used to determine the macroscopic outline of the tumor during stereotactic surgery[17]; the "molecular margin" of the tumor may be larger because the tumor diffusely infiltrates the surrounding tissues diffusely. In this way, tumor-targeted imaging has been used widely to visualize the molecular margin of a tumor during resection, and detect residual disease in the surgical bed.[14,18]

PET imaging offers a unique opportunity to refine delineation of the target volume precisely in patients with HNSCC, and to reduce damage to the surrounding normal tissues.[19] Conventional imaging methods and current response evaluation criteria in solid tumors are based mainly on morphological indicators to evaluate therapy efficacy (eg, tumor size). Molecular imaging is used to monitor the treatment response by visualizing expression of a specific molecule,[20] and maybe more sensitive and may occur earlier than morphologic changes in tumors.

Based on these advantages of targeted molecular imaging of HNSCC mentioned above, we summarized the specific imaging targets and their application in various imaging modalities for HNSCC.

Tumor Cell Targets for Molecular Imaging of HNSCC

Tumor cell targets that are expressed uniquely or overexpressed markedly in tumors were some of the earliest targets for the diagnosis and treatments of cancer. Although HNSCCs contain kinds of tumors from various origins, the histologic type is the same, which means that they have similar biological behavior (eg, tumor invasion, metastasis), phenotype as well as tumor biomarkers. Tumor cell targets in HNSCC, like epidermal growth factor receptor (EGFR), cluster of differentiation 44 variant 6 (CD44v6), and mesenchymal-epithelial transition factor (c-Met), are shown in Table 1.

Growth factor receptors

Growth factor receptors are transmembrane proteins that interact with growth factors such as epidermal growth factor (EGF), transforming growth factor (TGF), and hepatocyte growth factor (HGF). The ligand-receptor interaction activates downstream reactions, which leads to diverse biologic consequences, including cell proliferation, angiogenesis, and apoptosis inhibition. These receptors have been implicated in the targeted therapy and molecular imaging of HNSCC. Among them, the EGFR is overexpressed in HNSCC at high levels. Also, the EGFR has been the most widely used target for HNSCC imaging.

Epidermal Growth Factor Receptor

The EGFR is a transmembrane receptor tyrosine kinase overexpressed in up to 90% of HNSCCs.[21] The natural ligands of EGFR include EGF and TGFα. EGFR overexpression promotes tumor growth, invasion, metastasis, and angiogenesis.[22] High EGFR expression levels are closely related to a high risk of metastasis and poor prognosis in HNSCC.[21] Hence, the EGFR is an attractive target for molecular imaging of HNSCC.

Anti-EGFR monoclonal antibodies (mAbs) bind to EGFRs with high affinity, and have been used widely in the imaging of HNSCC. Anti-EGFR mAbs labeled with near-infrared (NIR) fluorophores have been investigated in HNSCC models. Rosenthal *et al*[23,24] showed that cetuximab and panitumumab labeled with cyanine 5.5 or IRDye800, respectively, can be used to identify residual tumor and regional lymph-node metastasis accurately, demonstrating that both are suitable for the intra-operative detection of HNSCC with fluorescence imaging (FI). Rosenthal *et al*[18,25] recently verified the high sensitivity and safety of IRDye800CW-labeled cetuximab for surgical navigation and identification of additional positive nodes in HNSCC patients. Their results showed that FI with IRDye800CW-labeled cetuximab (25 mg/m^2) yielded the highest sensitivity and specificity for the removal of metastatic lymph nodes and provided adequate contrast to identify metastatic lymph nodes *in situ* [Figure 1].[25] Other NIR fluorescent probes, such as anti-EGFR antibodies conjugated to quantum dots (QDs), have been investigated for imaging oral squamous cell carcinoma *in vivo*.[26]

Radionuclides have been conjugated with anti-EGFR mAbs for HNSCC imaging as well. Hoeben *et al*[27] found that single-photon emission CT (SPECT) with ^{111}In-labeled cetuximab revealed good tumor uptake in mice with human FaDu HNSCC xenografts. van Dijk and colleagues developed ^{111}In-labeled F(ab′)$_2$ fragments of cetuximab, which had rapid blood clearance and better tumor penetration than the whole immunoglobulin G did.[28] This tracer could be used to assess EGFR expression *in vivo* and possibly evaluate the treatment response to EGFR inhibition.[29] In a subsequent study, PET showed a clear increase in ^{111}In-cetuximab-F(ab′)$_2$ tumor uptake, but no change in fluorodeoxyglucose (^{18}F-FDG) uptake in irradiated mice bearing human SCCNij202 HNSCC xenografts [Figure 2A].[30] Similarly, van Dijk and colleagues found that PET showed significantly decreased ^{111}In-cetuximab-F(ab′)$_2$ tumor uptake in SCCNij202 HNSCC xenografts after treatment with cetuximab and a single 10-Gy dose of radiation, and

Table 1: Tumor cell targets and targeted imaging agents in HNSCC.

Targets and studies	Imaging method	Targeted imaging agent
Growth factor receptors		
EGFR		
Rosenthal *et al*, 2017, 2015[25,18]	FI	Cetuximab-IRDye800CW
Rosenthal *et al*, 2007[23]	FI	Cetuximab-Cy5.5
Yang *et al*, 2011[26]	FI	QD800-EGFR Ab
Knowles *et al*, 2012[89]	US	Anti-EGFR-targeted microbubbles
Colecchia *et al*, 2017[35]	MRI	EGF-coated magnetite nanoparticles
Melancon *et al*, 2011[36]	MRI	C225-SPIO@Au NS
Li *et al*, 2012[33]	PET	[^{18}F]FBEM-cEGF
Niu *et al*, 2009[32]	PET	^{64}Cu-panitumumab
Melancon *et al*, 2014[37]	SPECT	Apt-HAuNS
Hoeben *et al*, 2011[27]	SPECT	^{111}In-cetuximab
Van Loon *et al*, 2017[34]	PET/CT	^{89}Zr-cetuximab
Van Dijk *et al*, 2016[31]	PET/CT	^{64}Cu-cetuximab-F(ab′)$_2$
Van Dijk *et al*, 2014, 2013[28-31]	SPECT/CT	^{111}In-cetuximab-F(ab′)$_2$
c-MET		
Li *et al*, 2018[44]	PET	[^{18}F]FP-Met-pep1
Perk *et al*, 2008[45]	PET	^{89}Zr-DN30
Cell adhesion molecules		
CD44v6		
Borjesson *et al*, 2006[50]	PET	^{89}Zr-cmAb U36
Verel *et al*, 2003[49]	PET	U36-Df-^{89}Zr
Verel *et al*, 2002[48]	PET	^{186}Re-U36, ^{186}Re-BIWA4
Stroomer *et al*, 2000[52]	SPECT	^{99m}Tc-BIWA1
Colnot *et al*, 2000[51]	SPECT	^{186}Re-cmAb U36
Odenthal *et al*, 2018[53]	FI, SPECT/CT	^{111}In-DTPA-BIWA-IRDye800CW
Integrins		
Nieberler *et al*, 2018[56]	FI	Cy5.5-conjugated αvβ6-selective peptide
Roesch *et al*, 2018[57]	PET/CT	^{68}Ga-DOTA-SFLAP3
Atallah *et al*, 2016[58]	FI	Cy5-RAFT-c(-RGDfK-)$_4$
Yan *et al*, 2015[60]	SPECT/CT	^{99m}Tc-3P-RGD2
Wang *et al*, 2014[59]	MRI	Fmp-IO-Pc 4 nanoparticles
CD147		
Newman *et al*, 2008[61]	FI	Anti-CD147:Cy5.5
Knowles *et al*, 2012[89]	US	Anti-CD147-targeted microbubbles
EpCAM		
Van Driel *et al*, 2016[62]	FI	Anti-EpCAM/IRDye800CW
Other targets		
uPAR		
Christensen *et al*, 2017[16]	FI; PET	ICG-Glu-Glu-AE105;^{64}Cu-DOTA-AE105
Boonstra *et al*, 2017[65]	FI; SPECT	ATN658-ZW800-1; ^{111}In-ATN658
COX2		
Uddin *et al*, 2016[67]	FI	FA-NPs
Uddin *et al*, 2015[68]	FI	Fluorocoxib C
TfR		
Shan *et al*, 2008[72]	FI	Tf-NIR

HNSCC: Head and neck squamous cell carcinoma; EGFR: Epidermal growth factor receptor; FI: Fluorescence imaging; Cy 5.5: Cyanine 5.5; QD: Quantum dot; Ab: Antibody; US: Ultrasound; MRI: Magnetic resonance imaging; EGF: Epidermal growth factor; C225-SPIO@Au NS: Gold nanoshells encapsulated with superparamagnetic iron oxide and conjugated with a C225 monoclonal antibody (cetuximab); PET: Positron emission tomography; SPECT: Single-photon emission computed tomography; Apt-HAuNS: Aptamer-conjugated hollow gold nanospheres; CT: Computed tomography; [^{18}F]FP-Met-pep1: 4-nitrophenyl [^{18}F]-2-fluoropropionate-labeled mesenchymal-epithelial transition factor-binding peptide; CD44v6: Cluster of differentiation 44 variant 6; cmAb: Chimeric monoclonal antibody; ^{68}Ga-DOTA-SFLAP3: ^{68}Ga-labeled-DOTA sunflower trypsin latency-associated peptide 3; Cy 5: Cyanine 5; RAFT-c(-RGDfK-)$_4$: Regioselectivity addressable functionalized template-arginine-glycine-aspartic acid; RGD2: Arginine-glycine-aspartic acid 2; Fmp-IO-Pc 4 NPs: Fibronectin-mimetic peptide-conjugated iron oxide nanoparticles encapsulating photosensitizer Pc 4; EpCAM: Epithelial cell adhesion molecule; uPAR: Urokinase-like plasminogen activator receptor; ICG: Indocyanine green; COX2: Cyclooxygenase-2; FA-NPs: Fluorocoxib A-labeled poly(propylene sulfide)-b-poly[oligo(ethylene glycol) methyl ether acrylate; TfR: Transferrin receptor; Tf-NIR: Near-infrared fluorescent transferrin conjugate.

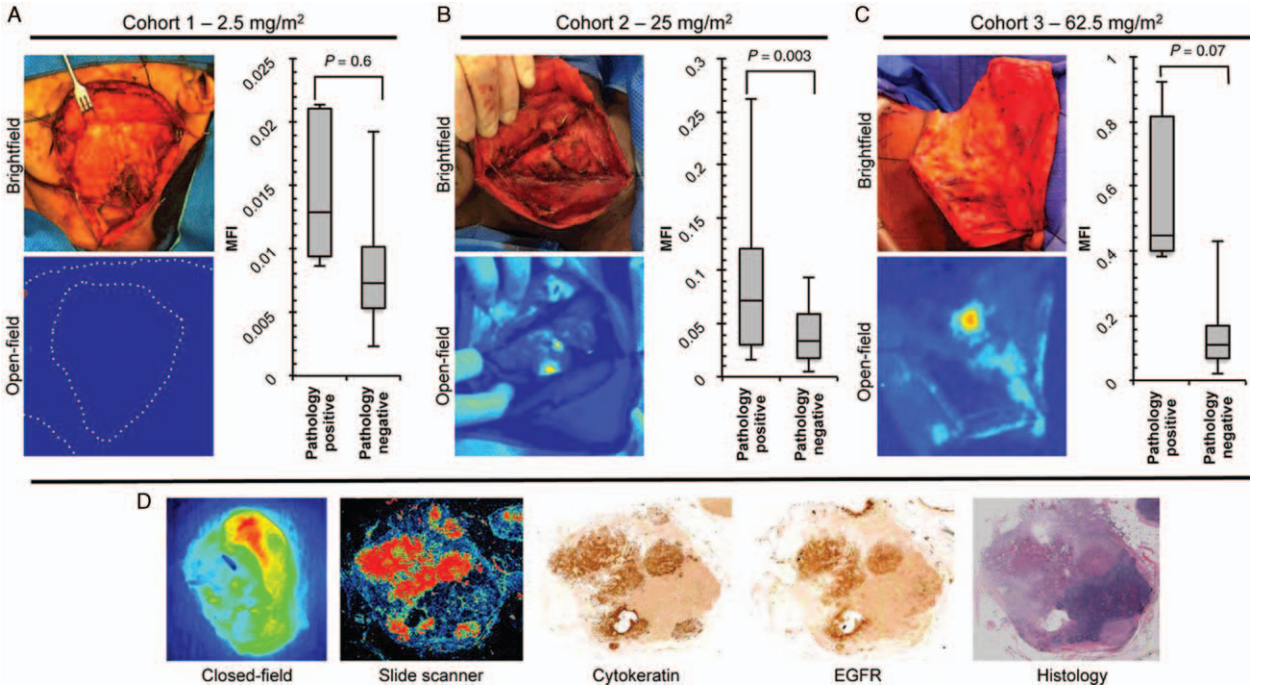

Figure 1: Intra-operative imaging of neck dissection. (A–C) Representative bright-field and open-field images and quantitative analyses of fluorescence in grossed lymph nodes for (A) cohort 1 (2.5 mg/m^2), (B) cohort 2 (25 mg/m^2), and (C) cohort 3 (62.5 mg/m^2). (Doses were based on the therapeutic dose of cetuximab 250 mg/m^2. Cohort 1 was given 1% of the therapeutic dose, cohort 2 received 10% of the therapeutic dose, and cohort 3 received 25% of the therapeutic dose.) (D) Representative closed-field image and fluorescence slide scanner acquisitions of grossed lymph nodes (left); matching immunohistochemical staining for cytokeratin and epidermal growth factor receptor (middle); and matching histopathological staining (right). EGFR: Epidermal growth factor receptor.

that ^{18}F-FDG uptake on PET correlated with tumor response in only the SCCNij202 model [Figure 2B].[20] van Dijk *et al*,[31] as well as Niu *et al*[32] and Li *et al*,[33] also demonstrated the potential of PET with ^{18}F- and ^{64}Cu-labeled tracers to image EGFR expression in HNSCC models. A recent phase-I trial of ^{89}Zr-labeled cetuximab in HNSCC demonstrated the clinical potential of such radiolabeled tracers.[34]

Owing to their multiple functions, nanoprobes targeting EGFRs have been synthesized for theranostic applications in HNSCC models. Researchers have used EGF-coated magnetite nanoparticles to image HN6 HNSCC. The nanoparticles accumulated in tumor tissues 24 to 48 h after intravenous injection, thereby demonstrating their potential for diagnostic applications [Figure 2C].[35] Melancon *et al*[36,37] developed two multifunctional nanoparticles, superparamagnetic iron oxide (SPIO) coated with gold nanoshells and ^{111}In-labeled hollow gold nanospheres, which were conjugated with EGFR-targeted mAbs or aptamers, respectively, to achieve diagnostic and therapeutic goals in oral cancer cells. As EGFR is also expressed in normal tissues, using EGFR-targeted imaging to assess the liver (one of the main metastatic sites of HNSCC) could be complicated.[38]

Mesenchymal-epithelial Transition Factor

c-Met is highly expressed in up to 80% HNSCC cases. c-Met is composed of an α chain and β chain linked via disulfide bonds.[39] c-Met is the sole receptor for HGF, and the deregulation of HGF/c-Met signaling promotes cell proliferation, migration, invasion, and angiogenesis in HNSCC.[39] Increased expression of c-Met is correlated significantly with regional lymph-node metastasis and a poor prognosis.[40] In addition to being a potential therapeutic target, c-Met may also be an imaging marker for tumors with high expression of c-Met.[41]

Researchers have shown the feasibility of PET and MRI with various agents targeting c-Met receptors in animal models of HNSCC and other cancers.[42-44] Perk *et al*[45] were the first to use PET to visualize the biodistribution of ^{89}Zr-labeled anti-c-Met mAbs in FaDu HNSCC xenografts. Recently, Li *et al*[44] showed a ^{18}F-labeled c-Met-binding peptide was suitable for PET imaging in mice bearing UM-SCC-22B HNSCC xenografts. Their investigation of the uptake, internalization, efflux *in vitro*, pharmacokinetics, and biodistribution of the targeted imaging probe [Figure 3A] showed great potential to visualize c-Met receptors for HNSCC with high expression of c-Met. Unfortunately, there was also non-specific uptake in the blood vessels.[46]

Cell adhesion molecules

Cell adhesion molecules are proteins located on the cell surface involved in binding with other cells or with the extracellular matrix (ECM). By doing so they trigger intracellular responses that affect intracellular signaling, cytoskeletal organization, and/or gene expression. Expression of some of them, such as CD44v6 and integrin αvβ6, is often upregulated in the oncogenesis of HNSCC, making them suitable imaging targets.

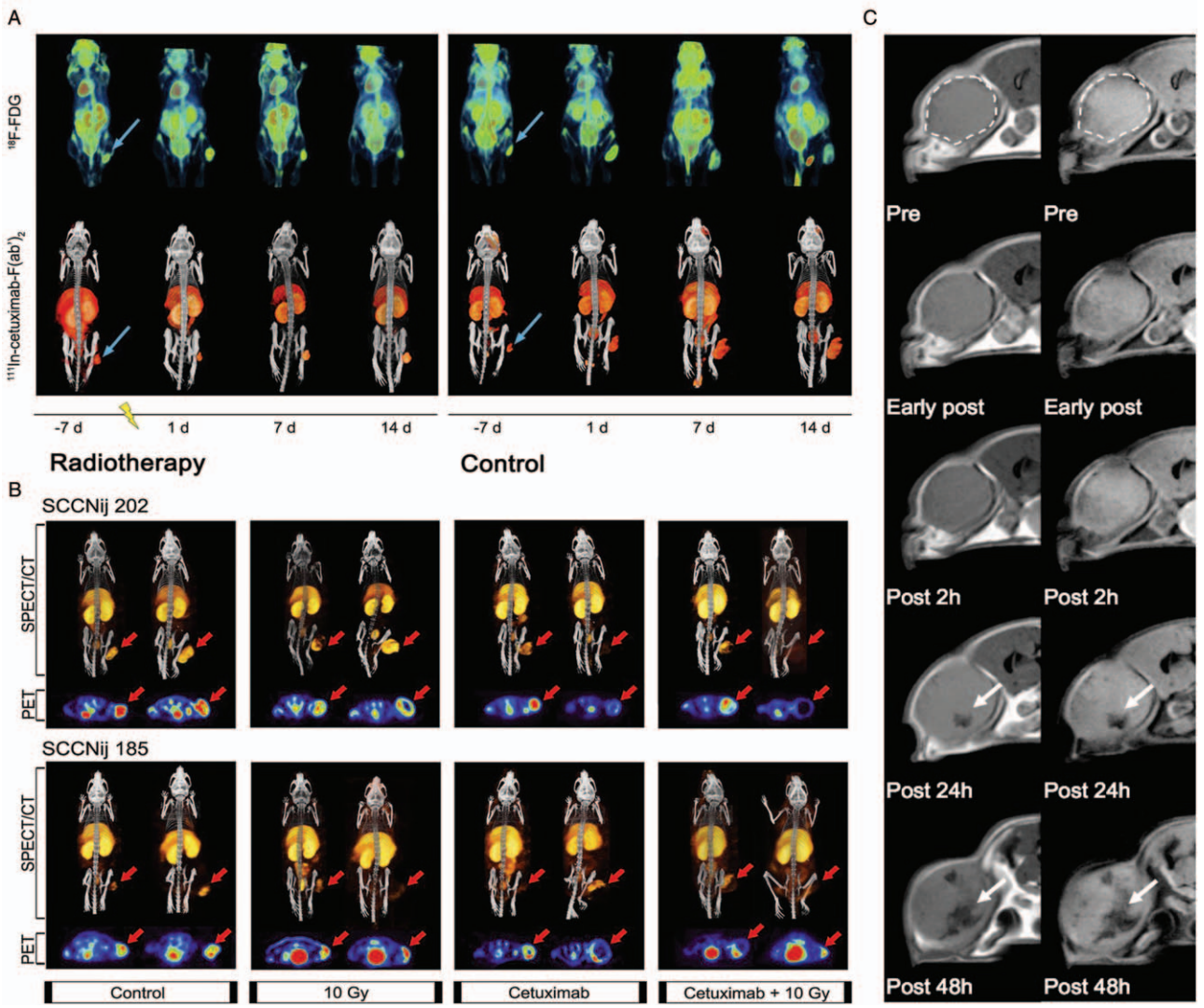

Figure 2: Epidermal growth factor receptor-targeted radionuclide imaging and MRI for evaluation of the treatment response and tumor localization, respectively. (A) Longitudinal visualization of irradiated and control SCCNij202 xenograft-bearing mice with ^{18}F-FDG PET and ^{111}In-cetuximab-F(ab′)$_2$ SPECT. SPECT and PET images were acquired after injection at 24 and 1 h, respectively. Tumors were irradiated at time 0 (indicated by the lightning bolt). Arrows indicate subcutaneous tumors in the right hind legs. (B) Tumor uptake of ^{111}In-cetuximab-F(ab′)$_2$ (SPECT dorsal view, 24 h after injection) and ^{18}F-FDG (PET transverse view, 1 h after injection) in mice bearing SCCNij202 xenografts (top row) and mice bearing SCCNij185 xenografts (bottom row). For each treatment group, images captured at baseline (10 days before treatment; left) and 18 days after treatment (right) are shown. Red arrows indicate tumors in right hind legs. SPECT images show background uptake in the liver, kidneys, and bladder, and PET images show background uptake in the bladder. (C) MRI with tumor-targeting nanoprobes *in vivo*. Representative T2- (left column) and T2* (right column)-weighted images obtained after intravenous injection of epidermal growth factor-conjugated magnetite nanoparticles (24 mg/kg) in a mouse bearing subcutaneous tumors. Arrows indicate areas of signal decline 24 and 48 h after injection. ^{18}F-FDG: Fluorodeoxyglucose; MRI: Magnetic resonance imaging; PET: Positron emission tomography; SPECT: Single-photon emission computed tomography.

Cluster of Differentiation 44 variant 6

CD44v6 is an oncogenic splice variant of the cell surface adhesion CD44.[38] CD44v6 overexpression has been documented in squamous cell carcinomas of the head and neck, lungs, and esophagus.[47,48] CD44v6 expression differs greatly between healthy and malignant tissue, which is a key advantage for molecular imaging.[38]

Anti-CD44v6 mAbs have been used widely for the imaging of preclinical models of HNSCC. ^{89}Zr-labeled U36 can be used to detect millimeter-sized tumors in animal models and lymph-node metastasis in HNSCC patients [Figure 3B].[49,50] Chimeric U36 labeled with ^{186}Re or ^{99}mTc has been used for the radioimmunodetection and radioimmunotherapy of HNSCC.[51] Stroomer *et al*[52] showed that another anti-CD44v6 mAb, BIWA1, has intermediate affinity for HNSCC in humans. Also, BIWA labeled with both IRDye800CW and ^{111}In could be used to detect HNSCC xenografts in nude mice accurately [Figure 3C], indicating that CD44v6 is a suitable target for FI-guided resection of invasive HNSCC.[53]

Integrins

Integrins play vital roles in cell adhesion, proliferation, survival, invasion, and migration by mediating cell-cell and cell-ECM interactions.[54] Integrins comprise non-covalent subunits (α and β), and combinations of different α and β subunits comprise different integrin heterodimers.[55] Among them, integrin αvβ6 has unique features. It is not expressed in healthy epithelia, but its expression is

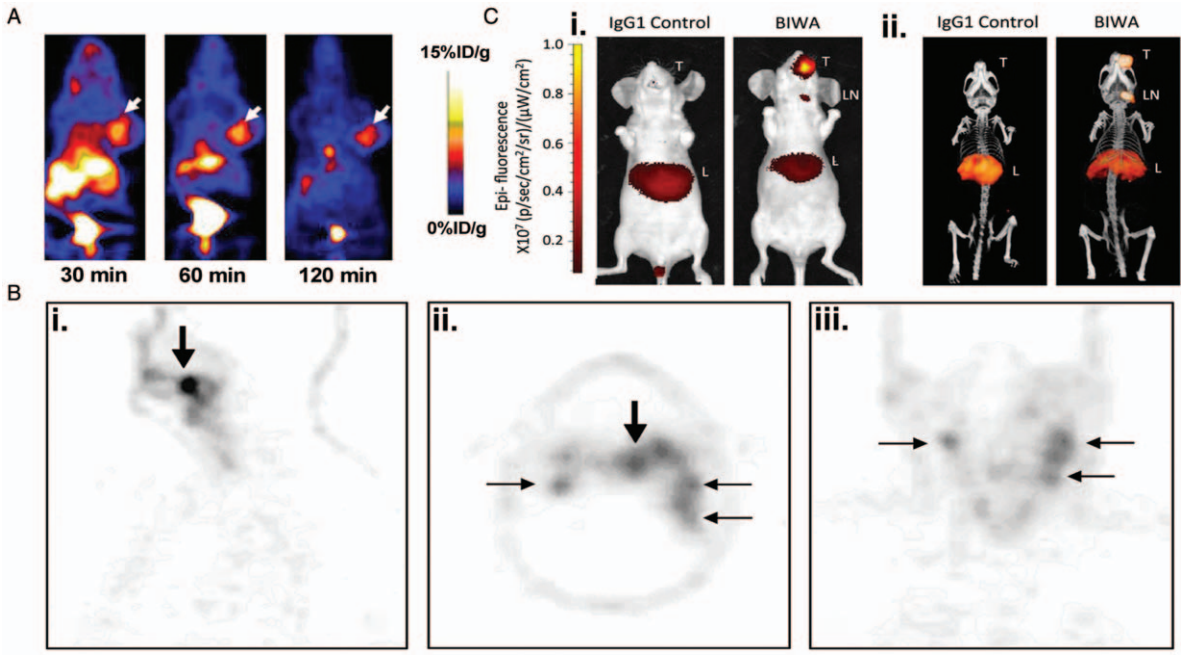

Figure 3: PET imaging with c-Met-targeted tracer in mice, and PET tracer or dual-modal imaging agent conjugated with anti-CD44v6 mAbs for detection of metastatic lymph nodes in an HNC patient and for HNSCC-xenografted mice, respectively. (A) Decay-corrected whole-body coronal microPET images of UM-SCC-22B tumor-bearing mice 30, 60, and 120 min after injection of 3.7 MBq (100 μCi) [^{18}F]FP-Met-pep1. Arrows indicate tumors on the right shoulders. (B) Immuno-PET with ^{89}Zr-labeled U36 shows a tumor in the left tonsil (large arrow) and lymph-node metastases (small arrows) at the left (levels II and III) and right (level II) side of the neck in an HNC patient. Sagittal (i), axial (ii), and coronal (iii) images were obtained 72 h after agent injection. (C) Whole-body NIR fluorescence images (i) and corresponding micro-SPECT/CT images (ii) show the biodistributions of ^{111}In-DTPA-BIWA-IRDye800CW and ^{111}In-DTPA-IgG1-IRDye800CW control antibody in HNSCC tumor-bearing mice 28 days and 72 h after intravenous injection of the agents. [^{18}F]FP-Met-pep1: 4-Nitrophenyl [^{18}F]-2-fluoropropionate-labeled mesenchymal epithelial transition-binding peptide; CD44v6: Cluster of differentiation 44 variant 6; c-Met: Mesenchymal-epithelial transition factor; CT: Computed tomography; IgG1: Immunoglobulin G1; LN: Lymph node; NIR: Near-infrared; HNC: Head and neck cancer; HNSCC: Head and neck squamous cell carcinoma; mAbs: Monoclonal antibodies; L: Liver; PET: Positron emission tomography; T: Tumor; SPECT: Single-photon emission computed tomography.

upregulated during tissue remodeling and carcinogenesis, making it a promising diagnostic and therapeutic target.[55,56] Integrins bind specifically to the arginine–glycine–aspartic acid (RGD) peptide sequence, so researchers have designed RGD-containing agents for targeted imaging. Recently, Roesch *et al*[57] demonstrated that the sunflower latency-associated peptide 3 was a promising tracer for the diagnostic imaging of HNSCC xenografts and patient tumors [Figure 4]. Other integrin subtypes have also been used for HNSCC imaging.[58-60]

Other cell adhesion molecules

Other cell adhesion molecules with potential use in the molecular imaging of HNSCC include CD147 and epithelial cell adhesion molecule (EpCAM). Newman *et al*[61] demonstrated that fluorescently labeled anti-CD147 antibody can be used for the clinical detection of HNSCC. EpCAM-specific NIR fluorescent agents have been used for intra-operative tumor delineation and resection in various animal models, including OSC19 orthotopic tongue tumor models.[62]

Other targets in tumor cells

Other targets in tumor cells have been utilized to image HNSCC including urokinase-like plasminogen activator receptor (uPAR), cyclooxygenase-2 (COX2), and the transferrin receptor (TfR). High expression of uPAR has been found in most carcinomas, including HNSCC,[63] whereas little uPAR is present in normal tissues and the dysplastic epithelium, thereby making uPAR a potential biomarker for targeted imaging.[64] uPAR-targeted multimodal imaging tracers have shown promising results in a preclinical model of HNSCC.[16,65] COX2 is expressed in only a few normal tissues, but high expression level of COX2 is found in inflammation and carcinogenesis.[66] A series of fluorescent COX2 inhibitors improved the signal-to-noise ratios in imaging studies of inflammatory lesions and early-stage human cancers expressing COX2,[67,68] thereby demonstrating their potential for targeted visualization of inflammatory disease and malignant tumors, including HNSCC.[69] The TfR is a cell membrane-internalizing receptor that is responsible for iron sequestration in mammalian cells.[70] It is overexpressed in malignant tumors, including HNSCC,[71] and a promising imaging target for head and neck cancer (HNC) imaging.[72]

Angiogenesis-Related Targets for Molecular Imaging of HNSCC

Angiogenesis is crucial for tumor growth, invasion, and metastasis. Accurate assessment of the angiogenic response to therapy would enable assessment of drug efficacy at a very early stage.[73] Therefore, angiogenesis imaging provides important information for treatment decisions. Potential angiogenesis-related targets for molecular imaging

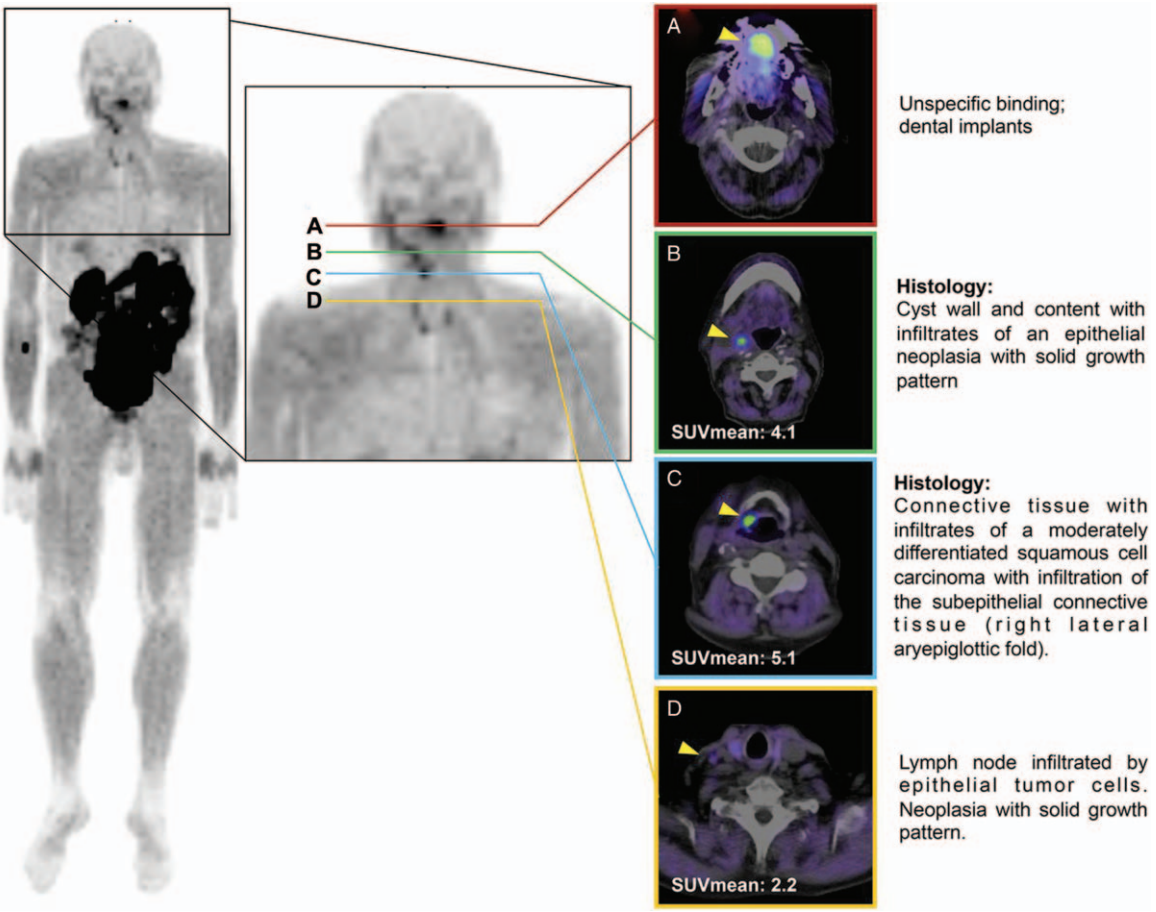

Figure 4: PET/CT images of an HNSCC patient after injection of 322 MBq ^{68}Ga-DOTA-SFLAP3. (A–D) Trans-axial slices of PET/CT fusion images. Yellow arrows indicate peptide accumulation. CT: Computed tomography; ^{68}Ga-DOTA-SFLAP3: ^{68}Ga-labeled-DOTA sunflower trypsin latency-associated peptide 3; HNSCC: Head and neck squamous cell carcinoma; PET: Positron emission tomography; SUV_{mean}: Mean standardized uptake value.

of HNSCC include integrins and vascular endothelial growth factor (VEGF) and its receptors (VEGFRs) [Table 2].

Integrin αvβ3

Integrin αvβ3 is expressed highly on the surface of tumor angiogenic vessel endothelial cells in almost all carcinomas.[74] Beer *et al*[75] showed that ^{18}F-labeled galacto-RGD can be used as a radiotracer for imaging αvβ3 expression; notably, this tracer has been used to identify integrin αvβ3 in the tumor neovasculature of HNSCC patients.[76] Chen *et al*[77] have developed a novel PET tracter, RGD-K5, that targets integrin αvβ3 to identify HNSCC patients with incomplete responses to concurrent chemoradiotherapy. Xie *et al*[78] prepared integrin αvβ3-targeting nanoshells that have good tumor-targeting ability and have been recognized as therapeutic nanoconstructs for effective cancer therapy. Terry *et al*[79] showed that SPECT with ^{111}In-labeled RGD2 can be used to clearly visualizes angiogenesis in FaDu and SCCNij202 HNSCC tumors. They co-injected the tracer with an excess of non-radiolabeled RGD2, which resulted in decreased tumor accumulation of the tracer, thus demonstrating the specificity of ^{111}In-labeled RGD2 *in vivo* [Figure 5].[79] RGD-conjugated QDs can target integrin αvβ3 specifically to generate clear fluorescence images of HNSCC tumors.[80] However, the problem is that endothelial cells also express integrin αvβ3, which leads to non-specific uptake of the imaging agents.

Table 2: Angiogenesis-related targets and targeted imaging agents in HNSCC.

Targets and studies	Imaging method	Targeted imaging agent
Integrin αvβ3		
Huang *et al*, 2013[80]	FI	QD800-RGD
Beer *et al*, 2006, 2007[75,76]	PET	^{18}F-galacto-RGD
Chen *et al*, 2016[77]	PET/CT	^{18}F-RGD-K5
Xie *et al*, 2011[78]	PET/CT	NS-RGDfK
Terry *et al*, 2014[79]	SPECT, SPECT/CT	^{111}In-RGD_2
VEGF		
Withrow *et al*, 2008[83]	FI	Bevacizumab-Cy5.5

FI: Fluorescence imaging; QD: Quantum dot; RGD: Arginine-glycine-aspartic acid; PET: Positron emission tomography; CT: Computed tomography; HNSCC: Head and neck squamous cell carcinoma; NS-RGDfK: Gold nanoshell conjugated with cyclo- arginine-glycine-aspartic acid-aspartic acid-phenylalanine-lysine; SPECT: Single-photon emission computed tomography; VEGF: Vascular endothelial growth factor; Cy 5.5: Cyanine 5.5.

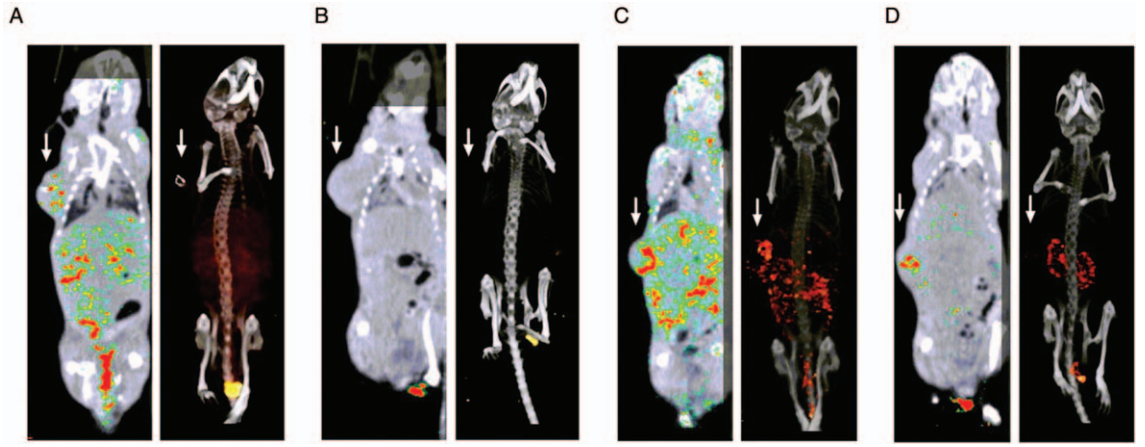

Figure 5: Imaging of tumor angiogenesis with ^{111}In-labeled RGD2 in FaDu and SCCNij202 HNSCC tumors. (A–D) Anterior two-dimensional (left) and three-dimensional (right) volume projections of fused SPECT/CT images of mice with subcutaneous FaDu (A and B) or SCCNij202 (C and D) xenografts on their right flanks. Mice were injected with either ^{111}In-RGD2 (A and C) or with ^{111}In-RGD2 plus cold excess (B and D). Static scans were recorded 1 h after injection. Arrows indicate tumor locations. CT: Computed tomography; RGD2: Arginine-glycine-aspartic acid 2; SPECT: Single-photon emission computed tomography.

VEGF and VEGFRs

VEGF plays an important role in angiogenesis; it is released by tumor cells and induces tumor neovascularization. VEGFRs are tyrosine kinases that function as key regulators of this process. VEGFRs are mediators of VEGF-induced angiogenesis, and their activation is related to cell proliferation and migration as well as the permeability and survival of the vascular endothelium.[81] For many cancers (including HNSCC), VEGF overexpression is an indicator of a poor prognosis,[82] which provides a basis for molecular imaging. A fluorescently labeled anti-VEGF Ab has been used to guide surgical resections in mice xenografted with HNSCC tumor cells.[83]

Modalities of Targeted Molecular Imaging of HNSCC

Optical molecular imaging

Optical molecular imaging is a rapidly developing method based on genomics, proteomics, and modern optical technology.[84] FI is one of the optical molecular imaging used most widely *in vivo*. Given its safety, high sensitivity, low cost, and real-time imaging, FI plays a vital role in the investigation of tumor occurrence, progression, and treatment response.[85] This modality has limitations: given the low energy of photons, optical molecular imaging has a limited depth of penetration (<2 cm); tissue autofluorescence can cause a significant background signal, thereby obscuring diagnostic information. These problems can be resolved partially by adapting NIR light, which can penetrate up to 10 cm deep into tissues. Moreover, tissue autofluorescence is negligible in the NIR region, which allows high-contrast imaging.[86] Therefore, NIR FI is investigated commonly in studies. QDs, whose main merits are photostability, good diffusion through solid tissue, and long-term excretion can also be a good choice for FI.[14]

US molecular imaging

US molecular imaging, namely contrast-enhanced ultrasound (CEUS), is achieved using targeted US contrast agents. A peptide, antibody, or other ligand designed to target a biomarker is conjugated on the shells of microbubble contrast agents. CEUS has several advantages, including its good temporal resolution, real-time imaging, wide availability, relative cost-effectiveness, portability, and no ionizing radiation. However, CEUS has some fundamental shortcomings: limited field of view, difficulty in quantifying signal, and dependence on operator expertise.[84] Furthermore, microbubbles are, in general, very large and are limited to intravascular molecular targets.[87] Thus, targets must be selected that are accessible to these microbubbles, and the attachment of microbubbles to the surface of endothelial cells must be strong enough for vascular areas where shear stress is high due to high blood velocity and viscosity.

Targeted microbubble contrast agents have been shown to improve the specific and sensitive depiction of molecular targets dramatically.[88] Knowles *et al*[89] also demonstrated the feasibility of US with CD147- and EGFR-targeting microbubbles for contrast-enhanced (ce) imaging of HNSCC *in vivo*.

Molecular MRI

MRI has several advantages, such as its relatively high temporal and spatial resolution, excellent tissue contrast and tissue penetration, no ionizing radiation, non-invasiveness, and simultaneous acquisition of anatomical structure and physiological function.[90] The two main kinds of molecular MRI contrast agents are ferromagnetic agents (negative contrast agents) and paramagnetic agents (positive contrast agents). The negative and positive contrast agents used most widely for molecular MRI are SPIO and gadolinium-diethylene triamine pentaacetic acid, respectively. These agents can be labeled with various ligands for tumor-specific imaging studies in HNSCC.[35,59] However, targeted MRI remains challenging for accurate detection of early-stage cancer due to the intrinsic low sensitivity of MRI. High-relativity molecular agents and higher field strengths may help improve its sensitivity.[84] In addition, it is critical

to select the cell-surface receptor to target because sufficiently high abundance can lead to more accumulation of contrast agents at the targeted site.

Radionuclide imaging

PET is the leading technique for routine targeted radionuclide molecular imaging in the clinic. Because of its superior sensitivity (10^{-11}–10^{-12} mol/L), limitless depth of penetration, and quantitative capabilities, PET plays critical roles in tumor detection, disease staging, and target volume delineation, evaluation of the therapy response and prognostic prediction.[91] Extensive preclinical trials have investigated the ability of PET to detect the expression of various target molecules on HNSCC tumor cells.[31,34,75] However, PET has some obvious shortcomings, including ionizing radiation, low geometric resolution (4–7 mm), and use of positron-emitting radionuclides.[92]

The spatial resolution of SPECT (8–10 mm) is lower than that of clinical PET (5–7 mm).[93] However, small-animal SPECT (micro-SPECT) has a higher spatial resolution than PET does, thereby making micro-SPECT more applicable to preclinical investigations.[94] In addition, SPECT can be used to undertake longitudinal studies since the radionuclides commonly available for SPECT have a longer half-life than those used for PET.[85]

Multimodality molecular imaging

As shown in Table 3, we compared the advantages and disadvantages of every imaging methods, and elucidate their application scope in current studies. But a single imaging modality can hardly meet the demands of individualized cancer diagnosis with the increasing trend toward the advancement of accurate diagnosis of diseases, especially cancer. Multimodality molecular imaging (in which different molecular imaging techniques are combined to take advantage of their strengths and compensate for their weaknesses) has been proposed for a long time and used for clinical diagnosis and treatments.[11,85] It can provide much more information for the accurate diagnosis of diseases.

PET/CT produces co-registered data that provide regions of increased ^{18}F-FDG accumulation on the PET image that correlate precisely with anatomic locations on the CT scan, thereby enhancing the accuracy of PET for the detection of lesions and delineating the target volume.[11] MRI has obvious advantages over CT, including its excellent soft-tissue contrast, high spatial resolution, and lack of ionizing radiation. ce PET/MRI has higher diagnostic efficiency for accurate conspicuity of lesions, infiltration of adjacent structures, and perineural spread in patients with HNC compared with cePET/CT.[95] An initial study revealed there were no significant differences among ^{18}F-FDG PET/MRI, ^{18}F-FDG PET/CT, and MRI in local tumor staging and cancer recurrence diagnosis.[96] Thus, further studies need to be conducted to demonstrate the potential value of PET/MRI in HNSCC patients. The development of dual-modality imaging radionuclide/optical imaging is also attractive [Figure 3C].

Despite its many benefits, multimodality molecular imaging has drawbacks: difficulties in improving and optimizing performance, creating reasonable combinations of different modalities, and developing multimodal contrast agents.[97]

Table 3: Characteristics and application of different molecular imaging modalities.

Imaging modalities	Advantages/disadvantages	Application in studies
Optical imaging	High sensitivity, low cost, and real-time monitoring; limited depth of penetration, significant background signal, cannot provide quantitative information	Human oral cavity (hard palate, tongue, buccal mucosa), cutaneous (temple, neck), lip, oropharynx (tonsil), piriform sinus[18,25]; subcutaneous/orthotopic tumor models*[23,26]
US	Good temporal resolution, real-time practice, widely availability, easy to operation, no ionizing radiation; limited field of view, difficulties in quantifying signal, and dependence on the expertise of the operator	Subcutaneous tumor model (human HNSCC cell line SCC-1)[89]
MRI	Excellent tissue contrast and tissue penetration, no ionizing radiation, anatomical/functional information; low sensitivity	Subcutaneous tumor model (human HNSCC cell line HN6, M4E)[35,59]
PET	High sensitivity, high resolution, quantitative; ionizing radiation, low geometric resolution, use of a positron emitting radionuclides	Human oropharynx SCC (tonsil, soft palate), oral cavity (tongue, floor of mouth, retromolar area, buccal), hypopharynx, larynx (glottic, supraglottic)[34,50,75,76]; xenograft models†[31-33]
SPECT	High sensitivity, quantitative; ionizing radiation, poor spatial resolution, use of emitting radionuclides	Oropharynx (tonsil), larynx (supraglottic, post-cricoid region), hypopharynx (piriform sinus), oral cavity (floor of mouth, tongue, retromolar area), neck[51,52]; tumor models‡[28-31]

*,†,‡Indicated the tumor models were established with various human HNSCC cell lines in relevant representative references. US: Ultrasound; HNSCC: Head and neck squamous cell carcinoma; SCC: Squamous cell carcinoma; MRI: Magnetic resonance imaging; PET: Positron emission tomography; SPECT: Single-photon emission computed tomography.

To ensure the biochemical process or information required will help to choose different combination of imaging modalities. Also, comprehensive expertise involving multidisciplinary cooperation (eg, medicine, biology, chemistry) is required to design a novel and feasible targeted multimodal contrast agent.

Conclusions

Targeted molecular imaging enables the dynamic, quantitative visualization of specific biochemical activity at cellular and molecular levels *in vivo*. This strategy aids development of personalized medicine for individual patients. Non-invasive visualization of a specific biological target *in vivo* relies on its interaction with the imaging probe. However, imaging agents with high affinity and specificity in this field are lacking. To overcome this difficulty, identification of optimal tumor targets/biomarkers, and design of imaging probes with improved targeting capabilities *in vivo* may be needed. Multimodality molecular imaging is also a promising way to provide more precise information for individual patients with HNSCC. We believe that with the persistent efforts of imaging specialists, more breakthroughs will be made in the near future.

Funding

This work was supported by grants from the National Scientific Foundation of China (No.91859202 and No. 81771901).

Conflicts of interest

None.

References

1. Santuray RT, Johnson DE, Grandis JR. New therapies in head and neck cancer. Trends Cancer 2018;4:385–396. doi: 10.1016/j.trecan.2018.03.006.
2. Argiris A, Karamouzis MV, Raben D, Ferris RL. Head and neck cancer. Lancet 2008;371:1695–1709. doi: 10.1016/s0140-6736(08)60728-x.
3. Miller KD, Siegel RL, Lin CC, Mariotto AB, Kramer JL, Rowland JH, *et al*. Cancer treatment and survivorship statistics, 2016. CA Cancer J Clin 2016;66:271–289. doi: 10.3322/caac.21349.
4. Du Y, Peyser ND, Grandis JR. Integration of molecular targeted therapy with radiation in head and neck cancer. Pharmacol Ther 2014;142:88–98. doi: 10.1016/j.pharmthera.2013.11.007.
5. Jameson JL, Longo DL. Precision medicine–personalized, problematic, and promising. New Engl J Med 2015;372:2229–2234. doi: 10.1056/NEJMsb1503104.
6. Jadvar H. Targeted radionuclide therapy: an evolution toward precision cancer treatment. AJR Am J Roentgenol 2017;209:277–288. doi: 10.2214/AJR.17.18264.
7. McDermott S, Kilcoyne A. Molecular imaging-its current role in cancer. QJM 2016;109:295–299. doi: 10.1093/qjmed/hcv141.
8. Rowe SP, Drzezga A, Neumaier B, Dietlein M, Gorin MA, Zalutsky MR, *et al*. Prostate-specific membrane antigen-targeted radiohalogenated PET and therapeutic agents for prostate cancer. J Nucl Med 2016;57 (Suppl 3):90s–96s. doi: 10.2967/jnumed.115.170175.
9. Hicks RJ. Citius, altius, fortius: an olympian dream for theranostics. J Nucl Med 2017;58:194–195. doi: 10.2967/jnumed.116.182188.
10. Patel SG, Shah JP. TNM staging of cancers of the head and neck: striving for uniformity among diversity. CA Cancer J Clin 2005;55:242–258. doi: 10.3322/canjclin.55.4.242.
11. Keshavarzi M, Darijani M, Momeni F, Moradi P, Ebrahimnejad H, Masoudifar A, *et al*. Molecular imaging and oral cancer diagnosis and therapy. J Cell Biochem 2017;118:3055–3060. doi: 10.1002/jcb.26042.
12. Economopoulou P, de Bree R, Kotsantis I, Psyrri A. Diagnostic tumor markers in head and neck squamous cell carcinoma (HNSCC) in the clinical setting. Front Oncol 2019;9:827. doi: 10.3389/fonc.2019.00827.
13. Mankoff DA, Link JM, Linden HM, Sundararajan L, Krohn KA. Tumor receptor imaging. J Nucl Med 2008;49 (Suppl 2):149S–163S. doi: 10.2967/jnumed.107.045963.
14. Nguyen QT, Tsien RY. Fluorescence-guided surgery with live molecular navigation–a new cutting edge. Nat Rev Cancer 2013;13:653–662. doi: 10.1038/nrc3566.
15. Hayashi M, Wu GS, Roh JL, Chang XF, Li XF, Ahn J, *et al*. Correlation of gene methylation in surgical margin imprints with locoregional recurrence in head and neck squamous cell carcinoma. Cancer 2015;121:1957–1965. doi: 10.1002/cncr.29303.
16. Christensen A, Juhl K, Persson M, Charabi BW, Mortensen J, Kiss K, *et al*. uPAR-targeted optical near-infrared (NIR) fluorescence imaging and PET for image-guided surgery in head and neck cancer: proof-of-concept in orthotopic xenograft model. Oncotarget 2017;8:15407–15419. doi: 10.18632/oncotarget.14282.
17. Kircher MF, de la Zerda A, Jokerst JV, Zavaleta CL, Kempen PJ, Mittra E, *et al*. A brain tumor molecular imaging strategy using a new triple-modality MRI-photoacoustic-Raman nanoparticle. Nat Med 2012;18:829–834. doi: 10.1038/nm.2721.
18. Rosenthal EL, Warram JM, de Boer E, Chung TK, Korb ML, Brandwein-Gensler M, *et al*. Safety and tumor specificity of cetuximab-IRDye800 for surgical navigation in head and neck cancer. Clin Cancer Res 2015;21:3658–3666. doi: 10.1158/1078-0432.CCR-14-3284.
19. Mena E, Thippsandra S, Yanamadala A, Redy S, Pattanayak P, Subramaniam RM. Molecular imaging and precision medicine in head and neck cancer. PET Clin 2017;12:7–25. doi: 10.1016/j.cpet.2016.08.009.
20. van Dijk LK, Boerman OC, Franssen GM, Kaanders J, Bussink J. In-111-cetuximab-F(ab ')(2) SPECT and F-18-FDG PET for prediction and response monitoring of combined-modality treatment of human head and neck carcinomas in a mouse model. J Nucl Med 2015;56:287–292. doi: 10.2967/jnumed.114.148296.
21. Kalyankrishna S, Grandis JR. Epidermal growth factor receptor biology in head and neck cancer. J Clin Oncol 2006;24:2666–2672. doi: 10.1200/JCO.2005.04.8306.
22. van Dijk LK, Boerman OC, Kaanders JH, Bussink J. PET imaging in head and neck cancer patients to monitor treatment response: a future role for EGFR-targeted imaging. Clin Cancer Res 2015;21:3602–3609. doi: 10.1158/1078-0432.CCR-15-0348.
23. Rosenthal EL, Kulbersh BD, King T, Chaudhuri TR, Zinn KR. Use of fluorescent labeled anti-epidermal growth factor receptor antibody to image head and neck squamous cell carcinoma xenografts. Mol Cancer Ther 2007;6:1230–1238. doi: 10.1158/1535-7160.MCT-06-0741.
24. Day KE, Sweeny L, Kulbersh B, Zinn KR, Rosenthal EL. Preclinical comparison of near-infrared-labeled cetuximab and panitumumab for optical imaging of head and neck squamous cell carcinoma. Mol Imaging Biol 2013;15:722–729. doi: 10.1007/s11307-013-0652-9.
25. Rosenthal EL, Moore LS, Tipirneni K, de Boer E, Stevens TM, Hartman YE, *et al*. Sensitivity and specificity of cetuximab-IRDye800CW to identify regional metastatic disease in head and neck cancer. Clin Cancer Res 2017;23:4744–4752. doi: 10.1158/1078-0432.CCR-16-2968.
26. Yang K, Zhang FJ, Tang H, Zhao C, Cao YA, Lv XQ, *et al*. In-vivo imaging of oral squamous cell carcinoma by EGFR monoclonal antibody conjugated near-infrared quantum dots in mice. Int J Nanomed 2011;6:1739–1745. doi: 10.2147/IJN.S23348.
27. Hoeben BA, Molkenboer-Kuenen JD, Oyen WJ, Peeters WJ, Kaanders JH, Bussink J, *et al*. Radiolabeled cetuximab: dose optimization for epidermal growth factor receptor imaging in a head-and-neck squamous cell carcinoma model. Int J Cancer 2011;129:870–878. doi: 10.1002/ijc.25727.
28. van Dijk L, Hoeben B, Kaanders J, Franssen G, Boerman O, Bussink J. Imaging of epidermal growth factor receptor expression in head and neck cancer with SPECT/CT and 111In-labeled cetuximab-F(ab')2. J Nucl Med 2013;54:2118–2124. doi: 10.2967/jnumed.113.123612.

29. van Dijk LK, Hoeben BAW, Stegeman H, Kaanders J, Franssen GM, Boerman OC, *et al*. In-111-cetuximab-F(ab ')(2) SPECT imaging for quantification of accessible epidermal growth factor receptors (EGFR) in HNSCC xenografts. Radiother Oncol 2013;108:484–488. doi: 10.1016/j.radonc.2013.06.034.
30. van Dijk LK, Boerman OC, Franssen GM, Lok J, Kaanders J, Bussink J. Early response monitoring with F-18-FDG PET and cetuximab-F (ab ')(2)-SPECT after radiotherapy of human head and neck squamous cell carcinomas in a mouse model. J Nucl Med 2014;55:1665–1670. doi: 10.2967/jnumed.114.141762.
31. van Dijk LK, Yim CB, Franssen GM, Kaanders J, Rajander J, Solin O, *et al*. PET of EGFR with Cu-64-cetuximab-F(ab)(2) in mice with head and neck squamous cell carcinoma xenografts. Contrast Media Mol Imaging 2016;11:65–70. doi: 10.1002/cmmi.1659.
32. Niu G, Li ZB, Xie J, Le QT, Chen XY. PET of EGFR antibody distribution in head and neck squamous cell carcinoma models. J Nucl Med 2009;50:1116–1123. doi: 10.2967/jnumed.109.061820.
33. Li WH, Niu G, Lang LX, Guo N, Ma Y, Kiesewetter DO, *et al*. PET imaging of EGF receptors using F-18 FBEM-EGF in a head and neck squamous cell carcinoma model. Eur J Nucl Med Mol Imaging 2012;39:300–308. doi: 10.1007/s00259-011-1969-8.
34. van Loon J, Even AJG, Aerts H, Ollers M, Hoebers F, van Elmpt W, *et al*. PET imaging of zirconium-89 labelled cetuximab: a phase I trial in patients with head and neck and lung cancer. Radiother Oncol 2017;122:267–273. doi: 10.1016/j.radonc.2016.11.020.
35. Colecchia D, Nicolato E, Ravagli C, Faraoni P, Strambi A, Rossi M, *et al*. EGFR-targeted magnetic nanovectors recognize, in vivo, head and neck squamous cells carcinoma-derived tumors. ACS Med Chem Lett 2017;8:1230–1235. doi: 10.1021/acsmedchemlett.7b00278.
36. Melancon M, Lu W, Zhong M, Zhou M, Liang G, Elliott A, *et al*. Targeted multifunctional gold-based nanoshells for magnetic resonance-guided laser ablation of head and neck cancer. Biomaterials 2011;32:7600–7608. doi: 10.1016/j.biomaterials.2011.06.039.
37. Melancon M. Selective uptake and imaging of aptamer- and antibody-conjugated hollow nanospheres targeted to epidermal growth factor receptors overexpressed in head and neck cancer. ACS Nano 2014;8:4530–4538. doi: 10.1021/nn406632u.
38. Spiegelberg D, Nilvebrant J. CD44v6-targeted imaging of head and neck squamous cell carcinoma: antibody-based approaches. Contrast Media Mol Imaging 2017;2017:2709547. doi: 10.1155/2017/2709547.
39. Rothenberger NJ, Stabile LP. Hepatocyte Growth factor/c-met signaling in head and neck cancer and implications for treatment. Cancers 2017;9:39. doi: 10.3390/cancers9040039.
40. Hartmann S, Bhola NE, Grandis JR. HGF/Met signaling in head and neck cancer: impact on the tumor microenvironment. Clin Cancer Res 2016;22:4005–4013. doi: 10.1158/1078-0432.CCR-16-0951.
41. Sun S, Liu S, Duan SZ, Zhang L, Zhou H, Hu Y, *et al*. Targeting the c-Met/FZD8 signaling axis eliminates patient-derived cancer stem-like cells in head and neck squamous carcinomas. Cancer Res 2014;74:7546–7559. doi: 10.1158/0008-5472.CAN-14-0826.
42. Pool M, van Scheltinga A, Kol A, Giesen D, de Vries EGE, Lub-de Hooge MN. Zr-89-onartuzumab PET imaging of c-MET receptor dynamics. Eur J Nucl Med Mol Imaging 2017;44:1328–1336. doi: 10.1007/s00259-017-3672-x.
43. Wu YW, Fan Q, Zeng F, Zhu JY, Chen J, Fan DD, *et al*. Peptide-functionalized nanoinhibitor restrains brain tumor growth by abrogating mesenchymal-epithelial transition factor (MET) signaling. Nano Lett 2018;18:5488–5498. doi: 10.1021/acs.nanolett.8b01879.
44. Li W, Zheng H, Xu J, Cao S, Xu X, Xiao P. Imaging c-Met expression using 18F-labeled binding peptide in human cancer xenografts. PLoS One 2018;13:e0199024. doi: 10.1371/journal.pone.0199024.
45. Perk LR, Stigter-van Walsum M, Visser GW, Kloet RW, Vosjan MJ, Leemans CR, *et al*. Quantitative PET imaging of Met-expressing human cancer xenografts with 89Zr-labelled monoclonal antibody DN30. Eur J Nucl Med Mol Imaging 2008;35:1857–1867. doi: 10.1007/s00259-008-0774-5.
46. Towner RA, Smith N, Doblas S, Tesiram Y, Garteiser P, Saunders D, *et al*. In vivo detection of c-Met expression in a rat C6 glioma model. J Cell Mol Med 2008;12:174–186. doi: 10.1111/j.1582-4934.2008.00220.x.
47. Orian-Rousseau V. CD44, a therapeutic target for metastasising tumours. Eur J Cancer 2010;46:1271–1277. doi: 10.1016/j.ejca.2010.02.024.
48. Verel I, Heider KH, Siegmund M, Ostermann E, Patzelt E, Sproll M, *et al*. Tumor targeting properties of monoclonal antibodies with different affinity for target antigen CD44V6 in nude mice bearing head-and-neck cancer xenografts. Int J Cancer 2002;99:396–402. doi: 10.1002/ijc.10369.
49. Verel I, Visser G, Boellaard R, Stigter-van Walsum M, Snow G, van Dongen G. 89Zr immuno-PET: comprehensive procedures for the production of 89Zr-labeled monoclonal antibodies. J Nucl Med 2003;44:1271–1281.
50. Borjesson PK, Jauw YW, Boellaard R, de Bree R, Comans EF, Roos JC, *et al*. Performance of immuno-positron emission tomography with zirconium-89-labeled chimeric monoclonal antibody U36 in the detection of lymph node metastases in head and neck cancer patients. Clin Cancer Res 2006;12:2133–2140. doi: 10.1158/1078-0432.CCR-05-2137.
51. Colnot DR, Quak JJ, Roos JC, van Lingen A, Wilhelm AJ, van Kamp GJ, *et al*. Phase I therapy study of 186Re-labeled chimeric monoclonal antibody U36 in patients with squamous cell carcinoma of the head and neck. J Nucl Med 2000;41:1999–2010.
52. Stroomer J, Roos J, Sproll M, Quak J, Heider K, Wilhelm B, *et al*. Safety and biodistribution of 99mTechnetium-labeled anti-CD44v6 monoclonal antibody BIWA 1 in head and neck cancer patients. Clin Cancer Res 2000;6:3046–3055. doi: 10.1093/carcin/21.8.1623.
53. Odenthal J, Rijpkema M, Bos D, Wagena E, Croes H, Grenman R, *et al*. Targeting CD44v6 for fluorescence-guided surgery in head and neck squamous cell carcinoma. Sci Rep 2018;8:10467. doi: 10.1038/s41598-018-28059-9.
54. Desgrosellier JS, Cheresh DA. Integrins in cancer: biological implications and therapeutic opportunities. Nat Rev Cancer 2010;10:9–22. doi: 10.1038/nrc2748.
55. Niu G, Chen X. Why integrin as a primary target for imaging and therapy. Theranostics 2011;1:30–47. doi: 10.7150/thno/v01p0030.
56. Nieberler M, Reuning U, Kessler H, Reichart F, Weirich G, Wolff KD. Fluorescence imaging of invasive head and neck carcinoma cells with integrin alphavbeta6-targeting RGD-peptides: an approach to a fluorescence-assisted intraoperative cytological assessment of bony resection margins. Br J Oral Maxillofac Surg 2018;56:972–978. doi: 10.1016/j.bjoms.2018.11.003.
57. Roesch S, Lindner T, Sauter M, Loktev A, Flechsig P, Muller M, *et al*. Comparison of the RGD motif-containing alphavbeta6 integrin-binding peptides SFLAP3 and SFITGv6 for diagnostic application in HNSCC. J Nucl Med 2018;59:1679–1685. doi: 10.2967/jnumed.118.210013.
58. Atallah I, Milet C, Henry M, Josserand V, Reyt E, Coll JL, *et al*. Near-infrared fluorescence imaging-guided surgery improves recurrence-free survival rate in novel orthotopic animal model of head and neck squamous cell carcinoma. Head Neck 2016;38:E246–E255. doi: 10.1002/hed.23980.
59. Wang D, Fei B, Halig L, Qin X, Hu Z, Xu H, *et al*. Targeted iron-oxide nanoparticle for photodynamic therapy and imaging of head and neck cancer. ACS Nano 2014;8:6620–6632. doi: 10.1021/nn501652j.
60. Yan B, Qiu F, Ren L, Dai H, Fang W, Zhu H, *et al*. (99m)Tc-3P-RGD2 molecular imaging targeting integrin alphavbeta3 in head and neck squamous cancer xenograft. J Radioanal Nucl Chem 2015;304:1171–1177. doi: 10.1007/s10967-015-3928-5.
61. Newman J, Gleysteen J, Barañano C, Bremser J, Zhang W, Zinn K, *et al*. Stereomicroscopic fluorescence imaging of head and neck cancer xenografts targeting CD147. Cancer Biol Ther 2008;7:1063–1070. doi: 10.4161/cbt.7.7.6109.
62. van Driel PBAA, Boonstra MC, Prevoo HAJM, van de Giessen M, Snoeks TJA, Tummers QRJG, *et al*. EpCAM as multi-tumour target for near-infrared fluorescence guided surgery. BMC cancer 2016;16:884. doi: 10.1186/s12885-016-2932-7.
63. Shi Z, Stack MS. Urinary-type plasminogen activator (uPA) and its receptor (uPAR) in squamous cell carcinoma of the oral cavity. Biochem J 2007;407:153–159. doi: 10.1042/BJ20071037.
64. Persson M, Skovgaard D, Brandt-Larsen M, Christensen C, Madsen J, Nielsen CH, *et al*. First-in-human uPAR PET: imaging of cancer aggressiveness. Theranostics 2015;5:1303–1316. doi: 10.7150/thno.12956.
65. Boonstra MC, Van Driel P, Keereweer S, Prevoo H, Stammes MA, Baart VM, *et al*. Preclinical uPAR-targeted multimodal imaging of locoregional oral cancer. Oral Oncol 2017;66:1–8. doi: 10.1016/j.oraloncology.2016.12.026.

66. Scheer M, Drebber U, Breuhahn K, Mockel C, Reuther T, Kern M, *et al*. Expression of cyclooxygenase-2 (COX-2) in an advanced metastasized hypopharyngeal carcinoma and cultured tumor cells. Oral Maxillofac Surg 2010;14:53–57. doi: 10.1007/s10006-009-0181-5.
67. Uddin MJ, Werfel TA, Crews BC, Gupta MK, Kavanaugh TE, Kingsley PJ, *et al*. Fluorocoxib A loaded nanoparticles enable targeted visualization of cyclooxygenase-2 in inflammation and cancer. Biomaterials 2016;92:71–80. doi: 10.1016/j.biomaterials.2016.03.028.
68. Uddin MJ, Crews BC, Ghebreselasie K, Daniel CK, Kingsley PJ, Xu S, *et al*. Targeted imaging of cancer by fluorocoxib C, a near-infrared cyclooxygenase-2 probe. J Biomed Opt 2015;20:50502. doi: 10.1117/1.JBO.20.5.050502.
69. Uddin MJ, Crews BC, Blobaum AL, Kingsley PJ, Gorden DL, McIntyre JO, *et al*. Selective visualization of cyclooxygenase-2 in inflammation and cancer by targeted fluorescent imaging agents. Cancer Res 2010;70:3618–3627. doi: 10.1158/0008-5472.CAN-09-2664.
70. Daniels TR, Delgado T, Helguera G, Penichet ML. The transferrin receptor part II: targeted delivery of therapeutic agents into cancer cells. Clin Immunol 2006;121:159–176. doi: 10.1016/j.clim.2006.06.006.
71. Kearsley JH, Furlong KL, Cooke RA, Waters MJ. An immunohistochemical assessment of cellular proliferation markers in head and neck squamous cell cancers. Br J Cancer 1990;61:821–827. doi: 10.1038/bjc.1990.184.
72. Shan L, Hao YB, Wang SP, Korotcov A, Zhang RS, Wang TX, *et al*. Visualizing head and neck tumors in vivo using near-infrared fluorescent transferrin conjugate. Mol Imaging 2008;7:42–49. doi: 10.2310/7290.2008.0006.
73. Hu XD, Xing LG, Yu JM. Nuclear medical molecular imaging of tumor angiogenesis: current status and future prospects. Chin Med J 2013;126:2741–2746. doi: 10.3760/cma.j.issn.0366-6999.20122591.
74. Hood JD, Cheresh DA. Role of integrins in cell invasion and migration. Nature Rev Cancer 2002;2:91–100. doi: 10.1038/nrc727.
75. Beer AJ, Haubner R, Wolf I, Goebel M, Luderschmidt S, Niemeyer M, *et al*. PET-based human dosimetry of 18F-galacto-RGD, a new radiotracer for imaging alpha v beta3 expression. J Nucl Med 2006;47:763–769.
76. Beer AJ, Grosu AL, Carlsen J, Kolk A, Sarbia M, Stangier I, *et al*. [18F]galacto-RGD positron emission tomography for imaging of alphavbeta3 expression on the neovasculature in patients with squamous cell carcinoma of the head and neck. Clin Cancer Res 2007;13:6610–6616. doi: 10.1158/1078-0432.CCR-07-0528.
77. Chen S, Wang H, Lin C, Chang J, Hsieh C, Liao C, *et al*. RGD-K5 PET/CT in patients with advanced head and neck cancer treated with concurrent chemoradiotherapy: results from a pilot study. Eur J Nucl Med Mol Imaging 2016;43:1621–1629. doi: 10.1007/s00259-016-3345-1.
78. Xie H, Diagaradjane P, Deorukhkar AA, Goins B, Bao A, Phillips WT, *et al*. Integrin alphavbeta3-targeted gold nanoshells augment tumor vasculature-specific imaging and therapy. Int J Nanomed 2011;6:259–269. doi: 10.2147/IJN.S15479.
79. Terry SY, Abiraj K, Lok J, Gerrits D, Franssen GM, Oyen WJ, *et al*. Can 111In-RGD2 monitor response to therapy in head and neck tumor xenografts? J Nucl Med 2014;55:1849–1855. doi: 10.2967/jnumed.114.144394.
80. Huang H, Bai Y-L, Yang K, Tang H, Wang Y-W. Optical imaging of head and neck squamous cell carcinoma in vivo using arginine-glycine-aspartic acid peptide conjugated near-infrared quantum dots. OncoTargets Ther 2013;6:1779–1787. doi: 10.2147/OTT.S53901.
81. Hamerlik P, Lathia JD, Rasmussen R, Wu Q, Bartkova J, Lee M, *et al*. Autocrine VEGF-VEGFR2-neuropilin-1 signaling promotes glioma stem-like cell viability and tumor growth. J Exp Med 2012;209:507–520. doi: 10.1084/jem.20111424.
82. Fang CY, Egleston BL, Ridge JA, Lango MN, Bovbjerg DH, Studts JL, *et al*. Psychosocial functioning and vascular endothelial growth factor in patients with head and neck cancer. Head Neck 2014;36:1113–1119. doi: 10.1002/hed.23421.
83. Withrow KP, Newman JR, Skipper JB, Gleysteen JP, Magnuson JS, Zinn K, *et al*. Assessment of bevacizumab conjugated to Cy5.5 for detection of head and neck cancer xenografts. Technol Cancer Res Treat 2008;7:61–66. doi: 10.1177/153303460800700108.
84. Turkbey B, Kobayashi H, Ogawa M, Bernardo M, Choyke PL. Imaging of tumor angiogenesis: functional or targeted? AJR Am J Roentgenol 2009;193:304–313. doi: 10.2214/AJR.09.2869.
85. Chen ZY, Wang YX, Lin Y, Zhang JS, Yang F, Zhou QL, *et al*. Advance of molecular imaging technology and targeted imaging agent in imaging and therapy. Biomed Res Int 2014;2014:819324. doi: 10.1155/2014/819324.
86. Bai M, Bornhop DJ. Recent advances in receptor-targeted fluorescent probes for in vivo cancer imaging. Curr Med Chem 2012;19:4742–4758. doi: 10.2174/092986712803341467.
87. Liang HD, Blomley MJ. The role of ultrasound in molecular imaging. Br J Radiol 2003;76:S140–S150. doi: 10.1259/bjr/57063872.
88. Bzyl J, Lederle W, Palmowski M, Kiessling F. Molecular and functional ultrasound imaging of breast tumors. Eur J Radiol 2012;81 (Suppl 1):S11–S12. doi: 10.1016/S0720-048X(12)70005-0.
89. Knowles J, Heath C, Saini R, Umphrey H, Warram J, Hoyt K, *et al*. Molecular targeting of ultrasonographic contrast agent for detection of head and neck squamous cell carcinoma. Arch Otolaryngol Head Neck Surg 2012;138:662–668. doi: 10.1001/archoto.2012.1081.
90. Gore JC, Manning HC, Quarles CC, Waddell KW, Yankeelov TE. Magnetic resonance in the era of molecular imaging of cancer. Magn Reson Imaging 2011;29:587–600. doi: 10.1016/j.mri.2011.02.003.
91. Afshar-Oromieh A, Malcher A, Eder M, Eisenhut M, Linhart HG, Hadaschik BA, *et al*. PET imaging with a [68Ga]gallium-labelled PSMA ligand for the diagnosis of prostate cancer: biodistribution in humans and first evaluation of tumour lesions. Eur J Nucl Med Mol Imaging 2013;40:486–495. doi: 10.1007/s00259-012-2298-2.
92. Wu Y, Briley K, Tao X. Nanoparticle-based imaging of inflammatory bowel disease. Wiley Interdiscip Rev Nanomed Nanobiotechnol 2016;8:300–315. doi: 10.1002/wnan.1357.
93. Blake P, Johnson B, VanMeter JW. Positron emission tomography (PET) and single photon emission computed tomography (SPECT): clinical applications. J Neuroophthalmol 2003;23:34–41. doi: 10.1097/00041327-200303000-00009.
94. Catafau AM, Bullich S. Molecular imaging PET and SPECT approaches for improving productivity of antipsychotic drug discovery and development. Curr Med Chem 2013;20:378–388. doi: 10.2174/0929867311320030009.
95. Kuhn FP, Hullner M, Mader CE, Kastrinidis N, Huber GF, von Schulthess GK, *et al*. Contrast-enhanced PET/MR imaging versus contrast-enhanced PET/CT in head and neck cancer: how much mr information is needed? J Nucl Med 2014;55:551–558. doi: 10.2967/jnumed.113.125443.
96. Varoquaux A, Rager O, Poncet A, Delattre BM, Ratib O, Becker CD, *et al*. Detection and quantification of focal uptake in head and neck tumours: (18)F-FDG PET/MR versus PET/CT. Eur J Nucl Med Mol Imaging 2014;41:462–745. doi: 10.1007/s00259-013-2580-y.
97. James ML, Gambhir SS. A molecular imaging primer: modalities, imaging agents, and applications. Physiol Rev 2012;92:897–965. doi: 10.1152/physrev.00049.2010.

How to cite this article: Wu J, Yuan Y, Tao XF. Targeted molecular imaging of head and neck squamous cell carcinoma: a window into precision medicine. Chin Med J 2020;133:1325–1336. doi: 10.1097/CM9.0000000000000751